MASSIVE BINARIES IN THE VICINITY OF Sgr A*

O. Pfuhl, T. Alexander, S. Gillessen, F. Martins, R. Genzel, F. Eisenhauer, T. Fritz, T. Ott

The Astrophysical Journal, 782:101 (10pp), 2014 February 20 doi:10.1088/0004-637X/782/2/101

MASSIVE BINARIES IN THE VICINITY OF Sgr A*[*]

O. Pfuhl[1], T. Alexander[2], S. Gillessen[1], F. Martins[3], R. Genzel[1,4], F. Eisenhauer[1], T. K. Fritz[1], and T. Ott[1]
[1] Max-Planck-Institut für Extraterrestrische Physik, D-85748 Garching, Germany; pfuhl@mpe.mpg.de
[2] Faculty of Physics, Weizmann Institute of Science, P.O. Box 26, Rehovot 76100, Israel
[3] LUPM, Université Montpelier 2, CNRS, Place Eugéne Bataillon, F-34095, Montpellier, France
[4] Department of Physics, University of California, Berkeley, CA 94720, USA
Received 2013 July 29; accepted 2014 January 4; published 2014 February 3

ABSTRACT

A long-term spectroscopic and photometric survey of the most luminous and massive stars in the vicinity of the supermassive black hole Sgr A* revealed two new binaries: a long-period Ofpe/WN9 binary, IRS 16NE, with a modest eccentricity of 0.3 and a period of 224 days, and an eclipsing Wolf–Rayet binary with a period of 2.3 days. Together with the already identified binary IRS 16SW, there are now three confirmed OB/WR binaries in the inner 0.2 pc of the Galactic center. Using radial velocity change upper limits, we were able to constrain the spectroscopic binary fraction in the Galactic center to $F_{\rm SB} = 0.30^{+0.34}_{-0.21}$ at a confidence level of 95%, a massive binary fraction close to that observed in dense clusters. The fraction of eclipsing binaries with photometric amplitudes $\Delta m > 0.4$ is $F_{\rm EB}^{\rm GC} = 3\% \pm 2\%$, which is consistent with local OB star clusters ($F_{\rm EB} = 1\%$). Overall, the Galactic center binary fraction seems to be similar to the binary fraction in comparable young clusters.

Key words: binaries: eclipsing – Galaxy: center – infrared: stars – stars: early-type – stars: massive – stars: Wolf–Rayet

Online-only material: color figures

1. INTRODUCTION

The Milky Way nuclear star cluster (NSC) is the closest galactic nucleus and therefore has been the target of detailed observations over the last few decades. It offers the unique possibility to resolve the stellar population and to study its composition and the dynamics close to a central black hole at an unrivaled level of detail. Precision astrometry of the innermost stars over almost two decades has proven the existence of a $4.3 \times 10^6\ M_\odot$ supermassive black hole (SMBH; Eisenhauer et al. 2005; Ghez et al. 2008; Gillessen et al. 2009).

Past studies of the Milky Way's NSC found that the stellar population can be divided into two classes: the cool and evolved giant stars and the hot and young main sequence/post–main sequence stars. While the bulk of the stellar population is >5 Gyr old (Pfuhl et al. 2011), the existence of the massive young stars is evidence for very recent star formation (Forrest et al. 1987; Allen et al. 1990). The most massive stars (WR/O stars) reside in a combination of a prominent warped disk, a second disklike structure highly inclined relative to the main disk, and a more isotropic component (Paumard et al. 2006; Lu et al. 2009; Bartko et al. 2009) at a projected distance of 0.″8–12″ from Sgr A* (1″ ≡ 0.04 pc, assuming a distance of $R_0 = 8.3$ kpc). The Galactic center (GC) disks must have formed in a rapid star burst ∼6 Myr ago (Paumard et al. 2006; Bartko et al. 2010), with a highly unusual initial mass function (IMF) that favored the formation of massive stars (Bartko et al. 2010; Lu et al. 2013). This extreme IMF deviates significantly from the standard Chabrier/Kroupa IMF with a power-law slope of $\alpha = -2.3$ (Kroupa 2001; Chabrier 2003) and seems to exist only in the vicinity of the SMBH. The extreme IMF is currently pictured as the result of an infalling gas cloud that settled in a disk around the SMBH. Compressional heating of the fragmenting disk due to the tidal field of the SMBH raised the gas temperature, leading to the formation of massive stars (Levin & Beloborodov 2003; Bonnell & Rice 2008). The fragmentation of an accretion disk, however, is not only expected to produce massive stars but also to favor the formation of binary systems (Alexander et al. 2008). Fast cooling (shorter than the orbital timescale of ≈1000 yr) in fragmenting self-gravitational disks leads to a dramatic increase in the formation of binaries. The simulations predict a fraction of multiple systems close to unity in that case.

Apart from the massive O-star disks, a second population of ordinary B stars can be found in the innermost 1″ around the SMBH, the so called S stars (Eisenhauer et al. 2005; Ghez et al. 2008; Gillessen et al. 2009). The origin of the S stars is a mystery. In situ formation seems impossible because of the strong tidal forces of the SMBH. On the other hand, inward migration from the greater GC area is limited by the short main sequence lifetime of only a few tens of megayears. This requires the stars to have formed not far from today's location. One of the currently favored mechanisms that explain the formation of the S stars is a three-body interaction of the SMBH and a binary system (Gould & Quillen 2003; Perets et al. 2007). The binary gets disrupted by the SMBH (Hills's mechanism; Hills 1988). The one companion is ejected and eventually ends as a hypervelocity star, while the other companion gets tightly bound to the SMBH.

Thus, the formation of both stellar populations is closely tied to the binarity of the massive O stars in the Galactic center. Although dynamical effects, like stellar capture or disruption due to stellar encounters, can change the initial binary fraction on timescales of only a few megayears (Sana et al. 2013), the detection of binaries in the Galactic center can constrain some of the formation models.

1.1. Observed Binary Fractions

The binary fraction of massive stars is the subject of intense studies. The detection difficulties of long-period and extreme-mass-ratio binaries makes it hard to estimate the true binary fraction and the underlying distribution of the binaries. Correlations or anticorrelations between cluster densities and binary

[*] Based on observations collected at the ESO Very Large Telescope (programs 075.B-0547, 076.B-0259, 077.B-0503, 179.B-0261 and 183.B-0100).

fractions have been suggested by various authors. An early study of García & Mermilliod (2001) concluded from measurements of OB clusters that the binary fraction decreases with increasing cluster density. More recent measurements by Mahy et al. (2009) revised the binary fractions of the clusters under study. Their results argue against a binary-density anticorrelation. Sana & Evans (2011) claim that variations of cluster binary fractions can be explained by statistical fluctuations due to small samples sizes. From theory an environment dependence of the binary fraction would be expected. Either through the initial conditions in the star-forming cloud that regulate the formation of multiple systems (e.g. Sterzik et al. 2003) or starting from a universal initial binary population, that is altered by dynamical evolution (Marks & Kroupa 2012). While in the first scenario the multiplicity only depends on the density of the cluster, the second scenario predicts that the multiplicity also depends on age.

Whether the cluster environment is reflected in the binary fraction, as suggested by theory, could not be definitely answered from the available observations. The most recent studies find spectroscopic binary fractions in OB clusters of 44% (Kiminki & Kobulnicky 2012), 51% (Sana et al. 2013), and up to 70% (Sana et al. 2012). Within the uncertainties, it seems that in OB clusters about half of the stars are binary systems.

For comparison, binaries among low-mass stars ($\approx 1\,M_{\odot}$) seem to be less frequent. Recent studies suggest binary fractions between 4% and 15% (Sollima et al. 2007; Sommariva et al. 2009) in old globular clusters. In less dense open clusters, Geller & Mathieu (2012) found 29% low-mass binaries. The field binary fraction is 57% (Duquennoy & Mayor 1991).

1.2. Binary Statistics

Studies of large OB associations, such as Cyg OB2, with hundreds of stars allowed the derivation of binary distribution statistics, namely, binary mass ratio, orbital separation, and eccentricity distributions. The observed distribution functions are found to be well described by power laws. Kobulnicky & Fryer (2007) and Kiminki & Kobulnicky (2012), for example, found a mass ratio $q = M_{\rm sec}/M_{\rm prim}$ distribution of $f(q) \propto q^{\alpha}$, with $\alpha = 0.1 \pm 0.5$, a log-period distribution of $f(\log P) \propto \log P^{\beta}$, with $\beta = 0.2 \pm 0.4$, and an eccentricity distribution of $f(e) \propto e^{\gamma}$, with $\gamma = -0.6 \pm 0.3$. A similar study of the Tarantula Nebula by Sana et al. (2013) found a somewhat steeper mass ratio, $\alpha = -1 \pm 0.4$, but also shorter periods, $\beta = -0.45 \pm 0.3$.

1.3. What Is Known about Binaries in the Galactic Center

Because of the large distance of the GC and the extreme extinction in the optical ($A_V > 30$; e.g., Fritz et al. 2011), the study of GC binaries is limited to the most massive early-type stars.

There is only one confirmed binary so far.

1. IRS 16SW consists of two equal 50 $M_{\odot}$ constituents, with a period of 19.5 days (Ott et al. 1999; Martins et al. 2007). The star is an eclipsing contact binary, which shows a large photometric and spectroscopic variability during its revolution.

However, a few more stars were speculated to be binaries.

1. IRS 8, a bow shock star about 30″ north of SgrA*, was speculated to be a binary because of its apparently young age of only 3 Myr (Geballe et al. 2006). No binary signature has been detected so far; however, the seemingly young age might be explained by the influence of a close companion on the primary evolution. We did not consider this star in our study because of its relatively large distance from the cluster center. Considering the steep radial profile of the early-type stars, it is not clear if IRS 8 can be associated with the WR disk formation.
2. IRS 7E2 is a massive Ofpe/WN9, where Paumard et al. (2001) reported a significant radial velocity change with respect to a previous measurement by Genzel et al. (2000). Unfortunately, we obtained only four additional epochs for that star. Among the few observations, we did not detect a significant radial velocity change. However, the star features very broad emission lines (FWHM = 1140 km s^{-1}), which show some intrinsic variability. Thus, to rule on the binarity of the star, more observations are required. So far, it can only be considered a binary candidate.
3. IRS 29N, a photometric variable, was interpreted by Rafelski et al. (2007) as the potential signature of a wind-colliding binary. However, older data from Ott et al. (1999) showed less variability and no periodicity. The star is classified as a dust-producing WC star (Paumard et al. 2006). Some irregular variability could thus be attributed to circumstellar dust. The stellar spectrum is very red and shows some extremely broad emission features. The width and the intrinsic variability of the features prevent a precise radial velocity measurement. Therefore, we were not able to confirm or rule out the binarity of IRS 29N.
4. Peeples et al. (2007) classified a photometrically variable star with a period of ∼42 days as an eclipsing binary candidate. As for IRS 8, the star is a relatively large distance (≈27″) from the cluster center and is therefore likely not related to the WR disk. Because of the large distance it was not included in our photometric and spectroscopic survey. However, its spectroscopic confirmation is a viable target for future observations.

2. OBSERVATIONS AND DATA PROCESSING

This work relies on spectroscopic and imaging data obtained at the Very Large Telescope (VLT) in Cerro Paranal, Chile, between 2003 and 2013. The observations were carried out under programs 075.B-0547, 076.B-0259, 077.B-0503, 087.B-0117, 087.B-0280, 088.B-0308, 288.B-5040, 179.B-0261, and 183.B-0100.

2.1. Imaging and Photometry

The photometric data were obtained with the adaptive optics camera NACO (Rousset et al. 2003; Lenzen et al. 2003). The photometric reference images were taken on the 2006 April 29 and on the 2010 March 31. We used the H- and Ks-band filters together with a pixel scale of 13 mas pixel^{-1}. To each image we applied sky subtraction, bad-pixel, and flat-field correction (Trippe et al. 2008). All images of good quality obtained during the same night were then combined into a mosaic with a field of view of $\approx 20'' \times 20''$. In total, we used 102 Ks-band images and 34 H-band images with temporal spacings from a few hours to 9 yr to construct light curves for a few thousand stars within the field of view.

2.2. Spectroscopy

Our spectroscopic data were obtained with the adaptive optics assisted integral field spectrograph SINFONI (Eisenhauer et al. 2003; Bonnet et al. 2004). In total, we used 45 observations

obtained between spring 2003 and summer 2013 with pixel scales between 50 × 100 and 125 × 250 mas. The data output of SINFONI consists of cubes with two spatial axes and one spectral axis. Depending on the plate scale, an individual cube covers 3.″2 × 3.″2 or 8″ × 8″; the spectral resolving power varies between 2000 and 4000 depending on the chosen bandpass and the field of view. We used the data reduction package SPRED (Schreiber et al. 2004; Abuter et al. 2006), including bad-pixel correction, flat fielding, and sky subtraction. The wavelength scale was calibrated with emission line gas lamps and fine-tuned on the atmospheric OH lines. Finally, we removed the atmospheric absorption features by dividing the spectra through a telluric spectrum obtained in each respective night.

2.3. Spectroscopic Sample Selection

Of the order of 200 early-type stars are known within 1 pc of Sgr A*. Their spectral types range from the most luminous O/WR stars with main sequence lifetimes of a few megayears to early B stars with main sequence lifetimes of several 10 Myr. Stars fainter than B dwarfs ($m_K > 16$) are too faint to be identified spectroscopically. Among the known early-type stars, we chose the brightest ones ($m_K < 12$) with prominent emission or absorption lines, which allowed a precise radial velocity measurement. We excluded stars with fit errors larger than 20 km s^{-1}. For instance, we excluded several bright WR stars with very broad wind emission lines. Our final sample consisted of 13 stars in close proximity to Sgr A*, which we repeatedly observed with SINFONI. Additionally, we used archival data from the same region, which gave us up to 45 independent observations per star (see Table 3). The observations cover period spacings between 1 day and 9 yr.

2.4. Velocity Measurement and Uncertainty

For the velocity measurement, we chose the most prominent spectral feature of each star. Depending on the spectral type, this was either the He I line at 2.059 μm, the He I line at 2.113 μm, or the Brγ line at 2.166 μm. The absolute velocity of the individual stars was measured by fitting a Gaussian. In order to detect relative velocity changes, we cross-correlated each spectrum with a reference spectrum of the same star. This provided significantly better velocity residuals and scatter than individual Gaussian fits. All velocities were corrected for the Earth's barycentric and heliocentric motion. The velocity uncertainties of the individual measurements are a combination of the fit errors, systematic errors (e.g., wavelength calibration), and intrinsic line variations of the stars. The formal fit errors in the best cases were as small as ≈2 km s^{-1}. However, this does not include systemic errors like wavelength calibration and drifts of the spectrograph. All stars in the sample are actually post–main sequence stars with typical wind emission profiles. The stars with the largest velocity fit errors were also those where the spectra clearly showed variability. This variability is typically associated with wind fluctuations. It can also be associated with binary wind interactions. In this case, the companion detection is difficult since the spectrum shows a complex interplay between reflex motion and binary wind interaction. To determine the overall velocity uncertainty (including systematics), we used three late-type stars contained in the integral field unit (IFU) fields and measured their velocities. Late-type giants are good spectroscopic references because they cannot have close companions (because of their physical size of a few astronomical units), and they show only slow pulsations. Thus, intrinsically, their radial velocities are thought to be very stable. Observationally, they are well suited because of their prominent absorption features in the K band, the CO band heads. The absorption shape allows a very precise radial velocity measurement (fit errors <2 km s^{-1}). It turns out that the late-type giants show a radial velocity scatter in our measurements of ∼6 km s^{-1} rms. We therefore estimate that our systematic errors are of that order. We attribute the differences between the fit errors on the observed velocity rms (Table 3) mainly to intrinsic nonperiodic line variations (except where a binary orbital solution was found; see the next section).

2.5. Binary Detection

We used a conservative approach and only identified stars as binaries where we could determine a significant orbital solution. In order to find periodic signals in the data, we calculated periodograms for each star in the sample. The sparse sampling, however, resulted in quite noisy periodograms. To identify significant peaks, we created 10^4 artificial periodograms from Gaussian noise data with the same time sampling as the stars. From the noise periodograms, we obtained a 3σ confidence region. Only peaks in the star periodograms lying above that confidence region were considered to be significant. As a result, only IRS 16NE showed a significant period of ∼222 days.

In a second step and in order to obtain an orbital solution and to check the robustness of the periodogram method, we tried to fit the data with binary orbits for a range of fixed periods. The orbit of a single line spectroscopic binary is defined by the period P, the eccentricity e, the systemic velocity γ, the longitude of periastron ω, the time of periastron T, and the mass function $f(m)$. However, fitting periodic functions such as a binary signature can be problematic, especially if one tries to fit the period. Often, the algorithm fails to converge or gets trapped in a local minimum. Therefore, we set the period as a prior and tried to fit the velocity curve of each star with the given prior period. We repeated the fitting for periods between 0.5 and 1000 days with a spacing of 1 day. We used the IDL fitting tool *MPFIT* (Markwardt 2009), which provided a fast fitting algorithm and which allowed defining parameter constrains. For stability reasons, we constrained the eccentricities $e < 0.98$. Although the period was set as a prior, we allowed the fitting routine to adjust the period by ±0.5 days with respect to the prior period. Thus, we could refine the crude 1 day period sampling. This resulted in a χ^2 distribution for the stated period range. Naturally, the period with the lowest χ^2 and the corresponding fit represents the best orbital solution. However, we only deemed solutions significant where the best χ^2 was reduced by at least a factor of 3 compared to the second-best solution. Out of the 12 stars in Table 3, again only IRS 16NE provided a significant orbital solution of 224 days, consistent with the most likely period from the periodogram method.

3. THE LONG-PERIOD BINARY IRS 16NE

The star IRS 16NE is the most luminous early-type star in the Galactic center ($m_H \approx 11.0$, $m_K \approx 9.2$). With a bolometric luminosity of $L \approx 2.2 \times 10^6\ L_\odot$ (Najarro et al. 1997; Martins et al. 2007) it is even one of the most luminous stars in the Milky Way. It is part of a young and massive population in the GC, thought to be luminous blue variables (LBVs; e.g., Paumard et al. 2001). Of the same type are stars IRS 16C, IRS 16NW, IRS 16SW, IRS 33E, and IRS 34W. IRS 16NE is at least 0.5 mag brighter than the other LBV stars (Paumard

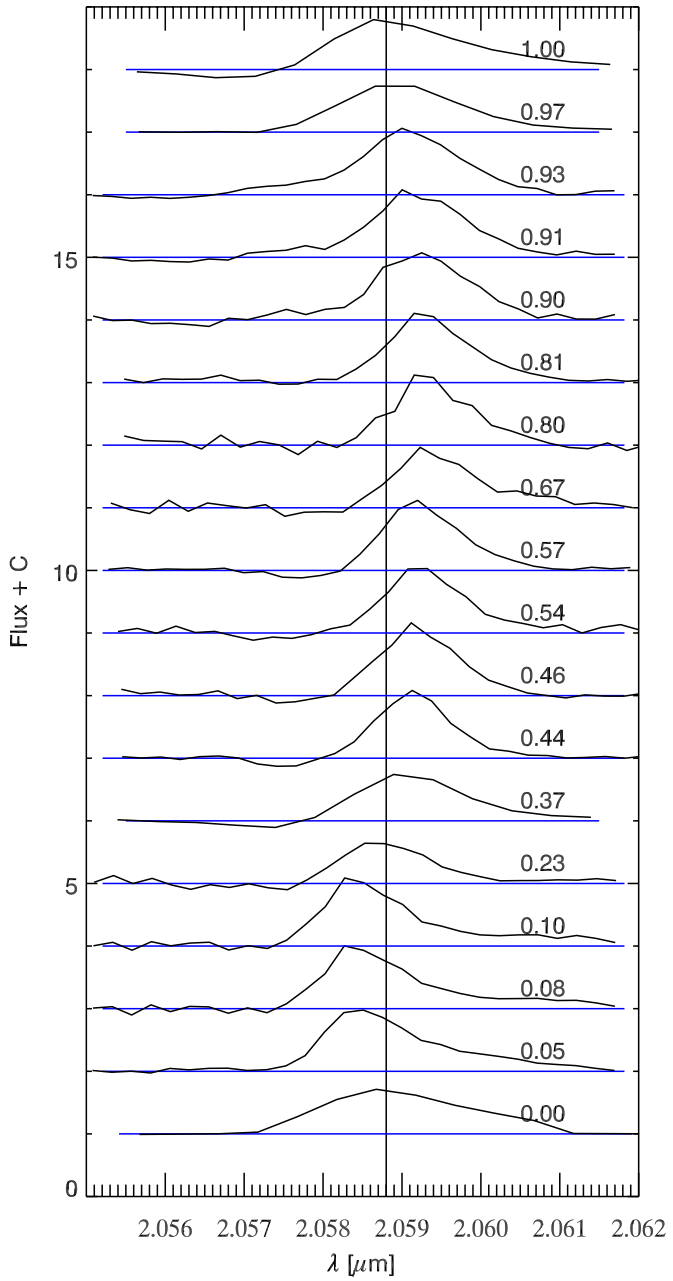

Figure 1. Sequence of spectra following one orbital period of IRS 16NE. The number indicates the period. The spectra have been corrected for the Earth barycentric motion. The solid line indicates the rest wavelength of He I (2.059 μm).

(A color version of this figure is available in the online journal.)

et al. 2006). LBVs are evolved massive stars that populate a region in the H-R diagram, where the luminosity approaches the Eddington luminosity, which leads to instabilities in their atmospheres. Therefore, those stars show strong variability in photometry and spectroscopy (Humphreys & Davidson 1994). Characteristic for this stellar phase are strong wind-driven mass loss and drastic changes in the stellar temperature and radius. Given that strong outbursts have not been observed yet for these six stars, they are thought to be LBVs in a stable phase (Martins et al. 2007).

Martins et al. (2006), Tanner et al. (2006), and Zhu et al. (2008) recognized a significant radial velocity change of IRS 16NE and speculated about a binary origin. However, they

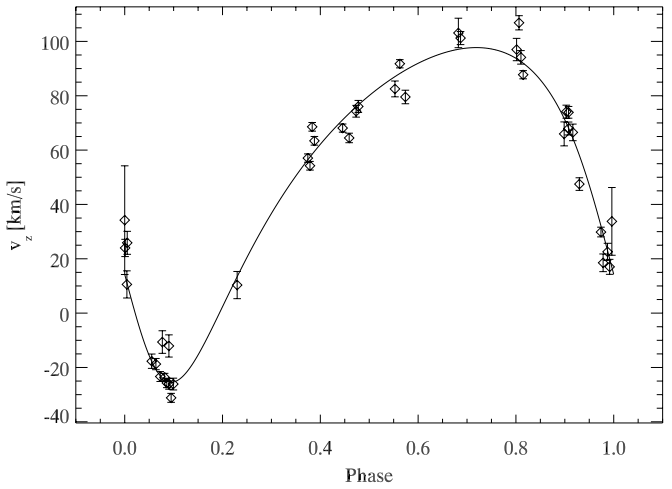

Figure 2. Radial velocity curve of IRS 16NE together with the best orbital solution (for $P = 224.09$ days and $e = 0.32$, solid line). The typical uncertainty on the radial velocity is ± 6.6 km s^{-1}. Parameters for the best-fit solution are given in Table 1.

were not able to deduce an orbital solution and deemed the star only a candidate.

After collecting another six years' worth of data and effectively doubling the number of observations, we can finally confirm the binarity of IRS 16NE.

3.1. Orbital Solution and Physical Parameters

We obtained 43 spectra of IRS 16NE, spread over roughly 10 yr with spacings of a few days up to years. It turned out that the orbit fitting (as described in Section 2.5) clearly favored a solution with a period of 224.09 days. The second-best period had a factor of 4 higher χ^2 than the best solution. A folded sequence of spectra covering one orbital period is shown in Figure 1. The orbit is clearly eccentric with $e = 0.32$. Figure 2 shows the folded radial velocity data together with the best-fit orbital solution. Since we were only able to measure the velocity of one companion, only the mass function,

$$f(m) = \frac{(M_2 \sin i)^3}{(M_1 + M_2)^2} = 4.58 \pm 0.17\, M_\odot$$

of the system could be determined (M_1 is the mass of the observed star, and M_2 is the mass of the unobserved star). However, the spectroscopic similarity of the primary star to the known eclipsing binary IRS 16SW argues for a primary mass close to 50 $M_\odot$. This means that the companion mass is $\geqslant 30\, M_\odot$. In the case of an edge-on orbit ($i = 90°$), the secondary mass is 30 $M_\odot$. A more massive companion requires a lower inclination. The lowest possible inclination is $\approx 46°$ for an equal-mass companion. In fact, a roughly equal-mass companion would explain the ≈ 0.5 mag excess of IRS 16NE compared to the other IRS 16 stars.

The binary IRS 16NE, with a semimajor axis of $a \sin i = 144\, \mu$as, will be a valuable test case for the upcoming second-generation Very Large Telescope Interferometer (VLTI) instrument GRAVITY. With its unprecedented $\approx 10\, \mu$as astrometric accuracy, it will be possible to determine the full orbital parameters of the system in less than 1 yr of observations.

4. ECLIPSING BINARIES

In order to find eclipsing binaries, we focused on the spectroscopically confirmed sample of early-type stars in the inner 10″

Table 1
Orbital Parameters as Derived from the Analysis of the Radial Velocity Curve

Parameter	Value
Semimajor axis, $a \sin i (10^6$ km)	179.1 ± 7.3
Eccentricity, e	0.32 ± 0.01
Systemic velocity, v_0 (km s^{-1})	52.45 ± 0.46
Semiamplitude $K1$ (km s^{-1})	61.57 ± 1.7
Longitude of periastron, ω (deg)	144.54 ± 1.65
Orbital period, P (days)	224.09 ± 0.09
Time of periastron, T (MJD)	52523.63 ± 1.47
$f(m)$ ($M_\odot$)	4.58 ± 0.17

Table 2
Orbital Parameters of the Eclipsing Binary E60

Parameter	Value
Separation, a ($R_\odot$)	22.6 ± 3
Eccentricity, e	≈ 0
Systemic velocity, v_0 (km s^{-1})	467 ± 10
Semi-amplitude $K1$ (km s^{-1})	150 ± 7
Inclination, i (deg)	70 ± 10
Orbital period, P (days)	2.276
Mass ratio, m	2 ± 0.5
$M_{\rm system}$ ($M_\odot$)	30 ± 10

around SgrA*. Among those stars, we selected those with average photometric errors <0.1 mag. That left us with 113 early-type stars within the field of view of the NACO 13 mas pixel^{-1} camera. We checked each of the light curves for variability. About half of the stars showed nonperiodic variability on a level of a few tenths of a magnitude as expected for OB stars (Lefèvre et al. 2009). In order to detect periodic variability, we used phase dispersion minimization (Stellingwerf 1978), a widely used technique in Cepheid and eclipsing binary searches. The inspection of the individual periodograms allowed us to identify two periodic variables with short periods (<100 days): the previously reported eclipsing binary IRS 16SW (Ott et al. 1999; Martins et al. 2007) with a period of 19.447 days and a new periodic variable with a period of 2.276 days.

4.1. The Eclipsing Binary E60

The new periodic star is the second reported eclipsing binary in the GC. Paumard et al. (2006) identified the star as a WN7 Wolf–Rayet type with $m_K = 12.4$, located at $\Delta\alpha = -4\farcs36$ and $\Delta\delta = -1\farcs65$ from Sgr A*. Following the nomenclature of Paumard et al. (2006), the star is referred to as E60. The back-folded H- and K-band light curve can be seen in Figure 3. The color-independent variability argues for an occultation event such as an eclipse of a companion. Variability due to pulsation or extinction from circumstellar dust typically leads to strong color changes. The WN7 star features broad emission lines, which results in relatively large radial velocity errors. Nonetheless, E60 shows a significant radial velocity change within days (only one companion is detectable). The radial velocity change is cophased with the photometric periodicity, as the back-folded radial velocity curve indicates (Figure 4). Using the available photometric and spectroscopic data, we tried to model the binary with the program Nightfall.[5] The near-sinusoidal light curve argues for a very close binary. In fact, to model the light curve, we had to use a Roche lobe filling factor of 1.1. This means that the companions are in contact. This is not surprising, given the short orbital period of only 2.276 days. Furthermore, the large photometric amplitude requires the inclination to be >60°. The mass and the mass ratio of the system are essentially determined by the radial velocity amplitude. Unfortunately, the few velocity measurements and the relatively large errors limit the ability to constrain those parameters. For a well-determined fit, we would require more spectroscopic epochs, especially with short time spacings of only a few hours. However, we found a reasonable solution (see Table 2) that can reproduce the observations.

We modeled the system with a total system mass of 30 $M_\odot$ and a mass ratio of 2. An uneven mass ratio is required because of the relatively low velocity change for the given orbital period and inclination. Thus, the primary mass is 20 $M_\odot$, and the secondary mass is 10 $M_\odot$. In fact, those masses are typical for evolved WR stars of similar brightness and spectral type WN7 (compare Table 2 in Martins et al. 2007). The stellar radii of WN7 stars inferred by Martins et al. (2007) are between 10 $R_\odot$ and 18 $R_\odot$, which matches the inferred binary contact separation of 22.6 $R_\odot$.

The binary E60 has a remarkably high systemic radial velocity of 422 ± 10 km s^{-1}. The proper motion of the system is 4.73 ± 0.14 mas yr^{-1} (T. K. Fritz 2013, private communication), which corresponds to 184 ± 6 km s^{-1} at the distance of the GC. Thus, the total systemic velocity is $v_{\rm 3D} = 460 \pm 12$ km s^{-1}. The velocity exceeds (2σ) the escape velocity ($v_{\rm esc} \approx 440$ km s^{-1}) at $4\farcs7$ projected distance from Sgr A*. The actual three-dimensional (3D) distance of E60 could be larger; that is, the escape velocity could be even lower. On the other hand, the absolute velocity of the star is probably less certain than the formal fit error might indicate. In particular, the strong wind lines of E60 could be biased by the actual wind morphology. In any case, the star seems to be at best marginally bound to Sgr A*.

5. DETERMINING THE SPECTROSCOPIC BINARY FRACTION

The observed spectroscopic binary fraction (2 out of 13 stars, IRS 16SW and IRS 16NE) represents only a lower limit to the true binary fraction. Note that the eclipsing binary E60 is not considered in the spectroscopic binary fraction. We had to exclude that star because our initial sample of stars that were repeatedly observed for the binarity study was chosen on the basis of the stars' small velocity fit error (obtained in an earlier single measurement). The binarity of E60 was only detected later because of its photometric variability. The radial velocity change was detected in archival data only after the photometric detection. In order to keep the spectroscopic sample unbiased, E60 therefore is not considered in the spectroscopic binary fraction.

Naturally, the probability of detecting a stellar companion depends on the primary mass, the secondary mass (i.e., the mass ratio q), the eccentricity e, and the orbital period P. It also depends on the number of observations, the radial velocity uncertainty, and how well the orbital period is sampled. To derive the true binary fraction, it is therefore necessary to take the detection incompleteness into account.

5.1. Companion Detection Probability

Thanks to the long-term monitoring of the stars in our sample, we were able to set tight constraints on the radial velocity changes of the respective stars. The masses of the

[5] The software was developed by R. Wichmann and is freely available at http://www.hs.uni-hamburg.de/DE/Ins/Per/Wichmann/Nightfall.html.

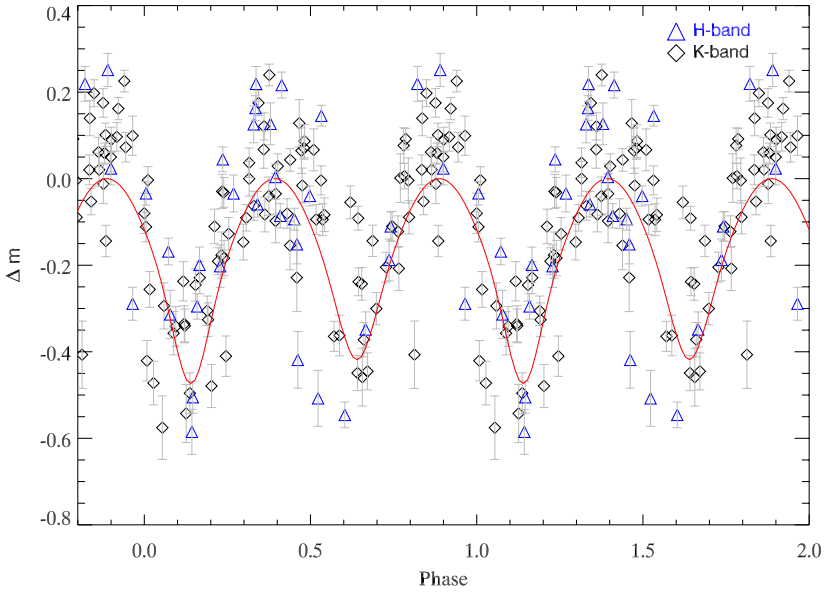

Figure 3. Back-folded *H*- and *K*-band light curve of the eclipsing binary E60. The orbital period is 2.276 days. Overplotted is a model light curve calculated with the free program Nightfall (for the parameters, see Table 2).

(A color version of this figure is available in the online journal.)

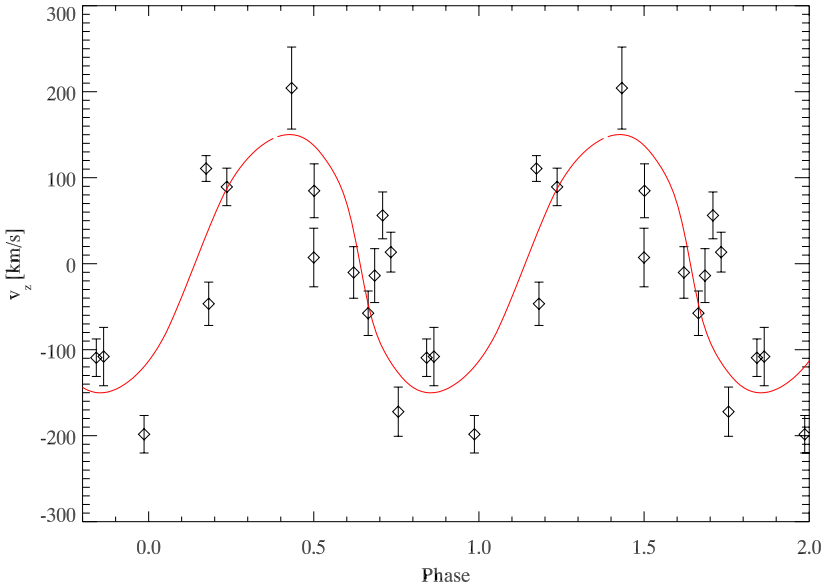

Figure 4. Measured radial velocities (the systemic velocity is subtracted) of the eclipsing binary E60. The broad wind lines of the star lead to relatively large velocity errors. Overplotted is the model radial velocity, which was calculated using the same model as in Figure 3.

(A color version of this figure is available in the online journal.)

stars can be quite well constrained from their luminosities and temperatures, i.e., the positions in the H-R diagram (e.g., Paumard et al. 2006; Martins et al. 2007). In order to determine the binary detection completeness, we used the assumption that the binaries in the Galactic center follow similar distribution functions as galactic and extragalactic OB clusters (described in Section 1.2). This assumption might seem somewhat arbitrary since it is not obvious that the distribution functions in disk star-forming regions are applicable to the special environment around a massive black hole. For lack of better alternatives and keeping this limitation in mind, we used the observed distribution functions for a Monte Carlo analysis.

For each star in the observed sample we created 10^4 artificial companions, where the mass ratio $0.1 < q < 1$, the eccentricity $0 < e < 0.9$, and the period $1 < P < 1000$ were drawn from the observed distribution functions (Section 1.2). The longitude ω, the time of periastron T, and the system inclination ($\cos i$) were drawn with uniform probability. Each companion realization resulted in an artificial radial velocity curve, which was sampled with the same time spacing as the actual observations. To account for the measurement uncertainties, we added random Gaussian noise with an rms equivalent to the systematic velocity uncertainty of 6 km s^{-1} (see Section 2.4) plus the fit error from Table 3 (added in squares). From the artificial discrete radial velocity points, we computed periodograms. As positive binary detections, we only accepted periodograms if the input period was correctly identified as the most prominent peak (within ±5%) and if the peak exceeded the confidence limit (defined in Section 2.5). We only accepted detections in our simulations with correctly identified periods. This seems to be

Table 3
Bright Early-type Stars Targeted in the Spectroscopic Survey

Id	sp Type[a]	N Data[b]	v_z (km s^{-1})	rms(v_z)[c] (km s^{-1})	Fit Error (km s^{-1})	M[d] ($M_\odot$)	$p_{\rm det}$[e] (Kiminki)	$p_{\rm det}$[f] (Sana)
IRS 16SW[g]	Ofpe/WN9	25	459.5	-	20	50	Binary	Binary
IRS 16NE	Ofpe/WN9	43	52.5	46.4	2.2	>40	Binary	Binary
IRS 16C	Ofpe/WN9	43	186	10.3	2.7	40	0.69	0.55
IRS 16NW	Ofpe/WN9	37	17	11.4	2.7	40	0.65	0.51
IRS 33E	Ofpe/WN9	42	214	10.1	3.6	40	0.70	0.55
IRS 34W	Ofpe/WN9	19	−184	6.5	2.3	25	0.37	0.37
IRS 13E2	WN8	23	−2	20.5	5.5	82.5	0.57	0.49
IRS 16SE2	WN5/6	38	191	15.4	6.5	17.2	0.59	0.49
IRS 29NE1	WC8/9	27	−99	27.5	19.8	25	0.40	0.32
IRS 33N (64)	B0.51 I	31	93	22.5	7.3	25	0.52	0.45
IRS 16CC	O9.5B0.5 I	35	145	27.1	8.5	40	0.58	0.48
IRS 16S (30)	B0.51 I	30	123	15.0	7.3	40	0.62	0.49
IRS 1E	B1-3 I	14	18	19.6	8.7	25	0.38	0.24

Notes.
[a] Spectral type taken from Paumard et al. (2006).
[b] Number of individual spectroscopic observations.
[c] Standard deviation of the N individual velocity measurements.
[d] Main-sequence masses are derived from the H-R diagrams of Paumard et al. (2006) and Martins et al. (2007).
[e] Companion detection probability determined with the distribution functions from Kiminki & Kobulnicky (2012; see Section 1.2).
[f] Companion detection probability determined with the distribution functions from Sana et al. (2013; see Section 1.2).
[g] Binary published in Martins et al. (2006).

justified because for the real data, we did not rely on only the periodogram method but actually tried to fit the data with a full orbital solution. Only stars where a unique orbital solution could be retrieved were accepted as binaries (Section 2.5). Therefore, the actual analysis went through a second filter. The computational cost of the fitting technique, however, prevented us from using it in the Monte Carlo analysis. On the basis of this cross-check, we assumed that the false-positive detections in the Monte Carlo analysis (without orbital solution because of computational cost) do not occur in the actual full data analysis. The number of identified binaries relative to the number of total trials was taken as the companion detection probability.

Table 3 states the detection probabilities for the stars in our sample. To check the robustness of the results, we ran the simulations with the two observed binary distribution functions of Sana et al. (2013) and Kiminki & Kobulnicky (2012). The Sana distribution features, on average, lower companion masses compared to the Kiminki study but also shorter periods. The stars with the lowest radial velocity rms have detection probabilities >0.7. In other words, the chance to have missed a companion is less than 0.3. Naturally, the detection probability can never reach unity simply because of the random inclination. Systems observed close to face on are not detectable. The sample stars with the largest radial velocity errors, low primary masses, or only a few observations have detection probabilities as low as 0.38. The average detection rate is 0.55 in the case of the Kiminki distribution and 0.45 in the case of the Sana distribution. Since we cannot tell which distribution function should be preferred for the Galactic center stars, we simply take the mean of the two results; that is, we obtain an average detection efficiency of $\langle p_{\rm det}\rangle = 0.50$.

5.2. Spectroscopic Binary Fraction

Assuming that all our sample stars intrinsically have the same probability to have a companion (the stars are all massive OB/WR stars), it is reasonable to use the average detection probability $\langle p_{\rm det}\rangle = 0.50$ (Table 3). The observed binary fraction (2 binaries out of 13 sources) is $F_{\rm obs} = 2/13 \approx 0.15$, which, after the correction for $p_{\rm det} < 1$, increases to $F_{SB} = F_{\rm obs}/p_{\rm det} \approx 0.30$. The distribution of binaries among the observed sources can be viewed as the outcome of a binomial process with probability P_{SB}, which is determined by the physics of binary formation. The detection-corrected binary fraction F_{SB} is then the sample estimator of P_{SB}. The confidence interval around it can be obtained in the small sample size limit by the Wilson score interval with continuity correction (Newcombe 1998; Brown et al. 2001). We thus find the 95% confidence interval to be $P_{SB} \in [0.09, 0.64]$, or $F_{SB} = 0.30^{+0.34}_{-0.21}$. The lower bound of the binary fraction is lower than the observed fraction. This takes into account that we could have been "lucky" in our choice of targets. While the uncertainties are quite large, we can exclude a binary fraction close to unity with high confidence. For example, $P_{SB} > 0.85$ is ruled out at the 99.999999% level.

6. ECLIPSING BINARY FRACTION

Estimating the true eclipsing binary fraction in the Galactic center is nontrivial because the detection probability depends strongly on the data sampling, the duration of the eclipse (i.e., the orbital separation and stellar radii), and the photometric amplitude (i.e., the inclination and relative sizes) of the system. However, we can compare the number of detected eclipsing binaries in the GC with the number of eclipsing binaries in local OB associations. We make the assumption that the binary E60, with an amplitude of $\Delta m_K \approx 0.45$ and average photometric error of $\sigma_K \approx 0.04$ mag, represents the detection limit. In the initial photometric sample of 113 early-type stars, 70 stars had photometric errors smaller than or equal to E60. Only one star showed greater photometric variability on short timescales, and that is IRS 16SW. Some of the other stars showed variability on an ∼0.1 mag level with no obvious

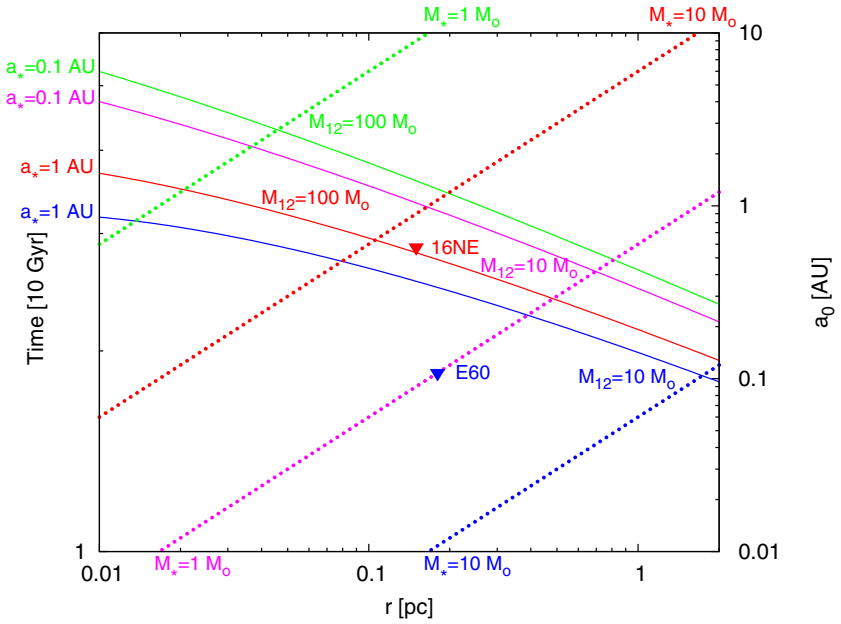

Figure 5. Tidal separation timescale T_t and the soft/hard critical semimajor axis a_0 as a function of distance for the MBH in the GC for very massive binaries ($M_{12} = 100\,M_\odot$) and moderately massive binaries ($M_{12} = 10\,M_\odot$). The tidal separation timescales (solid lines) are evaluated for $a_{12} = 0.1$ AU (of the order of that found for eclipsing binary E60) and $a_{12} = 1$ AU (of the order of that found for spectroscopic binary IRS16NE). The critical semimajor axes (dotted lines) are evaluated for the assumed mean stellar mass $\langle M_\star \rangle = 10\,M_\odot$, which is expected to be very close to the SMBH due to mass segregation (e.g., Alexander & Hopman 2009) or for a top heavy initial mass function (Alexander & Pfuhl 2014), and for $\langle M_\star \rangle = 1\,M_\odot$, as is expected farther out for a universal initial mass function. Approximate values for a_0 assuming $\langle M_\star \rangle = 10\,M_\odot$ are plotted for the binaries IRS 16NE ($r \sim 0.15$ pc, $M_{12} \sim 80\,M_\odot$, $a_{12} \sin i \simeq 1.2$ AU) and E60 ($r \sim 0.2$ pc, $M_{12} \sim 30\,M_\odot$, $a_{12} \simeq 0.1$ AU). These two binaries are close to their critical semimajor axes.

(A color version of this figure is available in the online journal.)

periodicity. Thus, out of the 70 stars, only 2, IRS16 SW and E60, are confirmed eclipsing binaries, i.e., $F_{\rm EB} = 3\% \pm 2\%$ (at 1σ confidence) with photometric amplitudes (>0.4 mag). The fraction of eclipsing binaries in local OB associations with similar amplitude variations $\Delta m \geqslant 0.4$ is $1.1\% \pm 0.3\%$ (out of ~2400 OB stars; see Lefèvre et al. 2009).

The deduced fraction of massive eclipsing binaries in the GC cannot have been altered significantly because of dynamical interaction, given the very recent formation (~6 Myr) of the massive stars and given the strong observational bias of eclipsing binaries to be tight, dynamically hard binaries (e.g., the soft/hard boundary for E60 would be $a \approx 300\,R_\odot$; Section 7), whereas eclipsing binaries typically have a of a few $10\,R_\odot$. However, very close binaries can interact through Roche lobe overflow, which can influence the stellar evolution. In this way, the binary fraction can be reduced after 6 Myr since the closest binaries have already interacted or even merged (Sana et al. 2013). Keeping this caveat in mind and despite the large Poisson errors, we conclude that the GC eclipsing binary fraction is close to the local value.

7. BINARY EVOLUTION IN THE GALACTIC CENTER

The evolution of binaries in dense galactic nuclei can be strongly modified by interactions with other stars and with the SMBH. We argue here that such effects will not significantly influence the observed properties and statistics of massive binaries in the GC. Disruption by the Galactic SMBH affects only the very small fraction of binaries that approach it within the tidal disruption radius, $r_t \simeq a_{12}(M_\bullet/M_{12})^{1/3}$, where $M_{12} = M_1 + M_2$ is the binary's total mass, a_{12} is its semimajor axis, and $M_\bullet$ is the SMBH mass. The timescale for the center of mass of a binary at radius r (assumed here to be of the order of the semimajor axis of its orbit around the SMBH) to be deflected, by stochastic two-body encounters with field stars, to an eccentric orbit that will lead to its tidal separation by the SMBH is $T_t \sim \log(2\sqrt{r/r_t})T_{\rm rlx}(r)$, where $T_{\rm rlx}$ is the two-body relaxation timescale and the log term reflects the typical time to diffuse in phase space into near-radial orbits with eccentricity $e_t = 1 - r_t/r$ (Frank & Rees 1976). The value of $T_{\rm rlx}$ in the GC, particularly whether it is longer or shorter than the age of the Milky Way (usually estimated by the Hubble time, $t_H = 10^{10}$ yr), depends on the yet unknown dynamical state of the inner parsec, in particular, whether it harbors a "dark cusp" of stellar remnants and faint stars (Alexander 2011). Estimates bracket it between $T_{\rm rlx}$ of a few 10^9 yr (Preto & Amaro-Seoane 2010) and a few 10^{10} yr (Merritt 2010). Given that $T_{\rm rlx} \sim \mathcal{O}(t_H)$ and that, typically, $\log(2\sqrt{r/r_t}) > 1$, tidal separation of binaries, especially short-lived massive ones, is negligible (Figure 5). Rapid angular momentum relaxation by resonant relaxation (Rauch & Tremaine 1996) is expected to become marginally relevant for this tidal separation only in the inner 0.01 pc (Hopman & Alexander 2006, Figure 7).

The binary's internal orbit also evolves stochastically because of the exchange of energy and angular momentum with field stars. The direction of the energy exchange, that is, whether, on average, the binary gains energy and becomes wider until it is disrupted ("evaporation") or whether it loses energy and shrinks until it coalesces, depends on its softness parameter s, defined as the ratio between its binding energy, $|E_{12}| = GM_1M_2/2a_{12}$, and the typical kinetic energy of the field stars, $E_K \sim \langle M_\star \rangle \sigma^2$, where $\sigma(r)$ is the one-dimensional (1D) velocity dispersion. Soft binaries with $s < 1$ will ultimately evaporate, while hard binaries with $s > 1$ will ultimately coalesce (Heggie 1975). In terms of the binary's semimajor axis, the soft/hard boundary is at the critical semimajor axis $a_0 = GM_1M_2/2\langle M_\star \rangle \sigma^2 \sim$

$(M_{12}^2/8M_\bullet\langle M_\star\rangle)r$, where the approximations $\sigma^2 \sim GM_\bullet/r$ (consistent with the results of Trippe et al. 2008) and $M_1 \sim M_2 \sim M_{12}/2$ are assumed. Figure 5 shows $a_0(r)$ for the very massive binaries with $M_{12} \sim \mathcal{O}(100\,M_\odot)$ and the moderately massive binaries with $M_{12} \sim \mathcal{O}(10\,M_\odot)$ that are relevant for this study. IRS16NE and E60 are close to their critical semimajor axes ($s \sim 1$). It is therefore unclear what direction their evolution would take, evaporation or coalescence. However, the evolutionary timescales will in any case be much longer than the binary's lifespan. A rough estimate of the time to coalescence is $T_c \sim \mathcal{O}([s_c - s]T_{\rm rlx})$, where s_c is the softness parameter where the binary's orbital decay is taken over by nondynamical effects (contact binary evolution or gravitational wave losses; not considered here), while the time to evaporation is $T_e \sim \mathcal{O}([\langle M_\star\rangle/M_{12}]sT_{\rm rlx})$ (Binney & Tremaine 1987; Alexander & Pfuhl 2014). It follows that as long as $0 \ll s \ll s_c$, dynamical binary evolution can be neglected for massive binaries in the GC.

These considerations do not apply for low-mass binaries, which are expected to undergo substantial evolution in the inner ~0.1 pc of the GC (e.g., Hopman 2009). A detailed study of the dynamical constraints that can be deduced from future detections of low-mass binaries in the GC is presented in T. Alexander et al. (2013, in preparation).

8. DISCUSSION

Our survey of more than a dozen massive OB/WR stars in the Galactic center revealed two previously unknown binaries, the long-period binary IRS 16NE and the eclipsing binary E60. Within the uncertainties, the spectroscopic binary fraction $F_{\rm SB} = 0.30^{+0.34}_{-0.21}$ in the GC seems to be within the uncertainty close to the fractions observed in other dense clusters (0.44–0.7). The same is true for the fraction of eclipsing binaries ($\Delta m \geqslant 0.4$) of $3\% \pm 2\%$, compared to 1% in other OB clusters. The fraction of multiple systems is significantly lower than unity. This is especially interesting since the multiplicity of stars formed in an SMBH accretion disk is regulated by the cooling timescale of the parental disk (Alexander et al. 2008). Fast cooling timescales ($t_{\rm cool} < t_{\rm dyn}$), which are believed to be present in black hole disks (e.g., Goodman 2003), lead to binary fractions close to unity and mainly equal-mass companions (Alexander et al. 2008). This is clearly not supported by our observations. The main caveat here is that the typical separations of binaries forming in an accretion disk might be significantly different from the separations observed in OB clusters. In this case, our study, which is most sensitive to small separations (periods less than a few hundred days), will underestimate the true binary fraction. The GC binary fraction cannot have been altered significantly by dynamical effects. Either massive binary systems in the GC are hard binaries, or the evolution timescale exceeds the age of the OB/WR disk (6 Myr). With an extraordinarily long period of 224 days, IRS 16NE is an example of a system that survived the dense cluster environment. The observed low binary fraction seems to be inconsistent with the current understanding of massive star formation in SMBH accretion disks. In that sense, the inferred binary fraction provides an additional constraint for future theoretical models that try to explain the formation of stars in the vicinity of SMBHs.

9. CONCLUSIONS

1. The massive 224 day long-period binary IRS 16NE is a rare system, even in environments less extreme than the Galactic center. Less than 10% of all known OB binaries have longer periods. The high mass of the binary constituents allows the large separation even in the dense cluster environment. The binary is dynamically hard, and it is therefore expected to survive dynamical evaporation.
2. We identified a new WR eclipsing binary (E60) at a distance of 4.″7 from Sgr A*. The system is a contact binary with a short period of only 2.3 days and a system mass of $M_{\rm prim} \approx 20\,M_\odot$ and $M_{\rm sec} \approx 10\,M_\odot$. Together with IRS 16SW, this star is the second known eclipsing binary in the Galactic center. The system has a remarkably high velocity of $v_{\rm 3D} \approx 460$ km s^{-1}, which is close to or even higher than the escape velocity at the radial distance from Sgr A*.
3. The spectroscopic binary fraction of the massive OB/WR stars in the Galactic center is $F_{\rm SB} = 0.30^{+0.34}_{-0.21}$, where the lower and upper limits represent the 95% confidence interval. This result is broadly consistent with the massive binary fraction observed in dense young clusters (see discussion in Section 1.1). It seems to be inconsistent with the current understanding of star formation in SMBH accretion disks, which predicts a binary fraction close to unity.
4. The eclipsing binary fraction ($\Delta m \geqslant 0.4$) in the GC is $3\% \pm 2\%$. Within the errors this is consistent with the fraction in other dense OB clusters (≈1%).

T.A. acknowledges support from ERC Starting grant No. 202996, DIP-BMBF grant No. 71-0460-0101, and Israel Science Foundation I-CORE grant No. 1829/12.

REFERENCES

Abuter, R., Schreiber, J., Eisenhauer, F., et al. 2006, NewAR, 50, 398
Alexander, R. D., Armitage, P. J., & Cuadra, J. 2008, MNRAS, 389, 1655
Alexander, T. 2011, in ASP Conf. Ser. 439, The Galactic Center: a Window to the Nuclear Environment of Disk Galaxies, ed. M. R. Morris, Q. D. Wang, & F. Yuan (San Francisco, CA: ASP), 129
Alexander, T., & Hopman, C. 2009, ApJ, 697, 1861
Alexander, T., & Pfuhl, O. 2014, ApJ, 780, 148
Allen, D. A., Hyland, A. R., & Hillier, D. J. 1990, MNRAS, 244, 706
Bartko, H., Martins, F., Fritz, T. K., et al. 2009, ApJ, 697, 1741
Bartko, H., Martins, F., Trippe, S., et al. 2010, ApJ, 708, 834
Binney, J., & Tremaine, S. 1987, Galactic Dynamics (Princeton, NJ: Princeton Univ. Press)
Bonnell, I. A., & Rice, W. K. M. 2008, Sci, 321, 1060
Bonnet, H., Abuter, R., Baker, A., et al. 2004, Msngr, 117, 17
Brown, L. D., Cal, T. T., & DasGupta, A. 2001, StaSc, 16, 101
Chabrier, G. 2003, PASP, 115, 763
Duquennoy, A., & Mayor, M. 1991, A&A, 248, 485
Eisenhauer, F., Abuter, R., Bickert, K., et al. 2003, Proc. SPIE, 4841, 1548
Eisenhauer, F., Genzel, R., Alexander, T., et al. 2005, ApJ, 628, 246
Forrest, W. J., Shure, M. A., Pipher, J. L., & Woodward, C. E. 1987, in AIP Conf. Ser. 155, The Galactic Center, ed. D. C. Backer (Melville, NY: AIP), 153
Frank, J., & Rees, M. J. 1976, MNRAS, 176, 633
Fritz, T. K., Gillessen, S., Dodds-Eden, K., et al. 2011, ApJ, 737, 73
García, B., & Mermilliod, J. C. 2001, A&A, 368, 122
Geballe, T. R., Najarro, F., Rigaut, F., & Roy, J.-R. 2006, ApJ, 652, 370
Geller, A. M., & Mathieu, R. D. 2012, AJ, 144, 54
Genzel, R., Pichon, C., Eckart, A., Gerhard, O. E., & Ott, T. 2000, MNRAS, 317, 348
Ghez, A. M., Salim, S., Weinberg, N. N., et al. 2008, ApJ, 689, 1044
Gillessen, S., Eisenhauer, F., Trippe, S., et al. 2009, ApJ, 692, 1075
Goodman, J. 2003, MNRAS, 339, 937
Gould, A., & Quillen, A. C. 2003, ApJ, 592, 935
Heggie, D. C. 1975, MNRAS, 173, 729
Hills, J. G. 1988, Natur, 331, 687
Hopman, C. 2009, ApJ, 700, 1933
Hopman, C., & Alexander, T. 2006, ApJL, 645, L133
Humphreys, R. M., & Davidson, K. 1994, PASP, 106, 1025

Kiminki, D. C., & Kobulnicky, H. A. 2012, ApJ, 751, 4
Kobulnicky, H. A., & Fryer, C. L. 2007, ApJ, 670, 747
Kroupa, P. 2001, MNRAS, 322, 231
Lefèvre, L., Marchenko, S. V., Moffat, A. F. J., & Acker, A. 2009, A&A, 507, 1141
Lenzen, R., Hartung, M., Brandner, W., et al. 2003, Proc. SPIE, 4841, 944
Levin, Y., & Beloborodov, A. M. 2003, ApJL, 590, L33
Lu, J. R., Do, T., Ghez, A. M., et al. 2013, ApJ, 764, 155
Lu, J. R., Ghez, A. M., Hornstein, S. D., et al. 2009, ApJ, 690, 1463
Mahy, L., Nazé, Y., Rauw, G., et al. 2009, A&A, 502, 937
Marks, M., & Kroupa, P. 2012, A&A, 543, A8
Markwardt, C. B. 2009, in ASP Conf. Ser. 411, Astronomical Data Analysis Software and Systems XVIII, ed. D. A. Bohlender, D. Durand, & P. Dowler (San Francisco, CA: ASP), 251
Martins, F., Genzel, R., Hillier, D. J., et al. 2007, A&A, 468, 233
Martins, F., Trippe, S., Paumard, T., et al. 2006, ApJL, 649, L103
Merritt, D. 2010, ApJ, 718, 739
Najarro, F., Krabbe, A., Genzel, R., et al. 1997, A&A, 325, 700
Newcombe, R. G. 1998, Statistics in Medicine, 17, 857
Ott, T., Eckart, A., & Genzel, R. 1999, ApJ, 523, 248
Paumard, T., Genzel, R., Martins, F., et al. 2006, ApJ, 643, 1011
Paumard, T., Maillard, J. P., Morris, M., & Rigaut, F. 2001, A&A, 366, 466
Peeples, M. S., Stanek, K. Z., & Depoy, D. L. 2007, AcA, 57, 173
Perets, H. B., Hopman, C., & Alexander, T. 2007, ApJ, 656, 709
Pfuhl, O., Fritz, T. K., Zilka, M., et al. 2011, ApJ, 741, 108
Preto, M., & Amaro-Seoane, P. 2010, ApJL, 708, L42
Rafelski, M., Ghez, A. M., Hornstein, S. D., Lu, J. R., & Morris, M. 2007, ApJ, 659, 1241
Rauch, K. P., & Tremaine, S. 1996, NewA, 1, 149
Rousset, G., Lacombe, F., Puget, P., et al. 2003, Proc. SPIE, 4839, 140
Sana, H., de Koter, A., de Mink, S. E., et al. 2013, A&A, 550, A107
Sana, H., de Mink, S. E., de Koter, A., et al. 2012, Sci, 337, 444
Sana, H., & Evans, C. J. 2011, in IAU Symp. 272, Active OB Stars: Structure, Evolution, Mass Loss, and Critical Limits, ed. C. Neiner, G. Wade, G. Meynet, & G. Peters (Cambridge: Cambridge Univ. Press), 474
Schreiber, J., Thatte, N., Eisenhauer, F., et al. 2004, in ASP Conf. Ser. 314, Astronomical Data Analysis Software and Systems (ADASS) XIII, ed. F. Ochsenbein, M. G. Allen, & D. Egret (San Francisco, CA: ASP), 380
Sollima, A., Beccari, G., Ferraro, F. R., Fusi Pecci, F., & Sarajedini, A. 2007, MNRAS, 380, 781
Sommariva, V., Piotto, G., Rejkuba, M., et al. 2009, A&A, 493, 947
Stellingwerf, R. F. 1978, ApJ, 224, 953
Sterzik, M. F., Durisen, R. H., & Zinnecker, H. 2003, A&A, 411, 91
Tanner, A., Figer, D. F., Najarro, F., et al. 2006, ApJ, 641, 891
Trippe, S., Gillessen, S., Gerhard, O. E., et al. 2008, A&A, 492, 419
Zhu, Q., Kudritzki, R. P., Figer, D. F., Najarro, F., & Merritt, D. 2008, ApJ, 681, 1254